



This discussion paper is/has been under review for the journal Atmospheric Chemistry and Physics (ACP). Please refer to the corresponding final paper in ACP if available.

Single particle characterization using the soot particle aerosol mass spectrometer (SP-AMS)

A. K. Y. Lee¹, M. D. Willis¹, R. M. Healy^{2,3}, T. B. Onasch⁴, and J. P. D. Abbatt¹

¹Department of Chemistry, University of Toronto, Toronto, Canada

²Department of Chemistry and Environmental Research Institute, University College Cork, Ireland

³Southern Ontario Centre for Atmospheric Aerosol Research, University of Toronto, Toronto, Canada

⁴Aerodyne Research, Inc., Billerica, Massachusetts, USA

Received: 14 May 2014 – Accepted: 29 May 2014 – Published: 12 June 2014

Correspondence to: A. K. Y. Lee (klee@chem.utoronto.ca)

Published by Copernicus Publications on behalf of the European Geosciences Union.

Single particle characterization

A. K. Y. Lee et al.

Title Page

Abstract

Introduction

Conclusions

References

Tables

Figures



Back

Close

Full Screen / Esc

Printer-friendly Version

Interactive Discussion



Abstract

Understanding the impact of atmospheric black carbon (BC) containing particles on human health and radiative forcing requires knowledge of the mixing state of BC, including the characteristics of the materials with which it is internally mixed. In this study, we demonstrate for the first time the capabilities of the Aerodyne Soot-Particle Aerosol Mass Spectrometer equipped with a light scattering module (LS-SP-AMS) to examine the mixing state of refractory BC (rBC) and other aerosol components in an urban environment (downtown Toronto). *K*-means clustering analysis was used to classify single particle mass spectra into chemically distinct groups. One resultant cluster is dominated by rBC mass spectral signals (C_1^+ to C_5^+) while the organic signals fall into a few major clusters, identified as hydrocarbon-like organic aerosol (HOA), oxygenated organic aerosol (OOA), and cooking emission organic aerosol (COA). A nearly external mixing is observed with small BC particles only thinly coated by HOA (~ 28 % by mass on average), while over 90 % of the HOA-rich particles did not contain detectable amounts of rBC. Most of the particles classified into other inorganic and organic clusters were not significantly associated with BC. The single particle results also suggest that HOA and COA emitted from anthropogenic sources were likely major contributors to organic-rich particles with low to mid-range aerodynamic diameter (d_{va}). The similar temporal profiles and mass spectral features of the organic clusters and the factors from a positive matrix factorization (PMF) analysis of the ensemble aerosol dataset validate the conventional interpretation of the PMF results.

1 Introduction

Atmospheric black carbon (BC) particles play an important role in regional air quality and introduce large uncertainties into radiative forcing estimates of the Earth's atmosphere (Bond et al., 2013). Processes such as fossil fuel combustion and biomass burning are the primary sources of ambient BC. Coatings on BC aerosol surfaces

Single particle characterization

A. K. Y. Lee et al.

Title Page

Abstract

Introduction

Conclusions

References

Tables

Figures



Back

Close

Full Screen / Esc

Printer-friendly Version

Interactive Discussion



**Single particle
characterization**

A. K. Y. Lee et al.

Title Page

Abstract

Introduction

Conclusions

References

Tables

Figures



Back

Close

Full Screen / Esc

Printer-friendly Version

Interactive Discussion



with widely varying morphology and thickness have been observed using electron microscopy (China et al., 2013, 2014). These coatings can be formed through condensation and coagulation of low-volatility materials co-emitted from combustion sources (e.g., unburned organics) and produced via photochemical processing during transport. Current research is evaluating whether particle coatings can significantly enhance the light absorption efficiency of ambient BC (Cappa et al., 2012; Jacobson, 2001; Lack et al., 2012; Metcalf et al., 2013). Also, coating materials can modify the hygroscopicity and/or the cloud activation of BC particles, thus affecting their atmospheric lifetime (McMeeking et al., 2011; Tritscher et al., 2011; Wang et al., 2010; Zhang et al., 2008). Improving our understanding of the mixing state of BC and the characteristics of its associated coatings is crucial to evaluate the fate and environmental impacts of ambient BC.

Real-time, quantitative single particle detection is necessary to determine the mixing state of ambient particles. In particular, the single particle soot photometer (SP2, DMT, Inc.) has been developed to quantify refractory BC (rBC) using single particle incandescence signals (Baumgardner et al., 2004; Stephens et al., 2003). Combining both optical scattering and incandescence signals, the SP2 has been used to evaluate the degree of mixing (internal vs. external) and estimate the coating thickness of BC particles in both field and laboratory studies (e.g., Metcalf et al., 2013; Moteki and Kondo, 2007; Schwarz et al., 2006; Shiraiwa et al., 2007, 2010). However, this instrument cannot characterize the chemical nature of the coating materials. Single particle mass spectrometry utilizing laser desorption/ionization methods such as the aerosol time-of-flight mass spectrometer (ATOFMS, TSI, Inc.) or particle analysis by laser mass spectrometry (PALMS) are powerful techniques, which provide rich size-resolved chemical information to examine the mixing state of both refractory (e.g., dust and BC) and non-refractory components in ambient particles (Pratt and Prather, 2012 and references therein). However, these single particle mass spectrometry techniques are number concentration-based methods and the associated pulsed laser desorption and ionization process makes particle mass quantification challenging (Pratt and Prather, 2012).

Single particle
characterization

A. K. Y. Lee et al.

Title Page

Abstract

Introduction

Conclusions

References

Tables

Figures



Back

Close

Full Screen / Esc

Printer-friendly Version

Interactive Discussion



In contrast, the Aerodyne Aerosol Mass Spectrometer (AMS, Aerodyne Research Inc.) separates the particle vaporization and ionization steps to make quantification of particulate mass possible, with different versions of the AMS deployed to measure mass concentrations and size distributions of non-refractory particulate matter (NR-PM) (e.g., Canagaratna et al., 2007; Drewnick et al., 2005; Jimenez et al., 2009; Ng et al., 2010; Zhang et al., 2007). Specifically, the application of positive matrix factorization (PMF) analysis to AMS measurements is well developed for source apportionment of organic aerosol and evaluation of aerosol aging (Lanz et al., 2007; Ng et al., 2010; Ulbrich et al., 2009; Zhang et al., 2011). A few previous studies have demonstrated that a time-of-flight AMS in conjunction with a light scattering module (LS-ToF-AMS) can be used to characterize ambient particles on a single particle basis, which allows investigation of the mixing state of NR-PM (Cross et al., 2009; Freutel et al., 2013; Liu et al., 2013). Different particle categorization approaches have been developed to analyze single particle datasets from the LS-ToF-AMS, including principle component analysis (Cross et al., 2009), *k*-means clustering analysis (Liu et al., 2013) and a classification algorithm based on comparison with reference mass spectra (Freutel et al., 2013). However, the LS-ToF-AMS is only able to detect non-refractory aerosol species that vaporize at $\sim 600^\circ\text{C}$.

The utility of the AMS was recently extended by development of the Soot-Particle Aerosol Mass Spectrometer (SP-AMS), which is able to quantify and characterize rBC and NR-PM simultaneously (Cross et al., 2010; Onasch et al., 2012). An infrared (IR) laser vaporizer has been incorporated into the standard high resolution time-of-flight AMS (HR-ToF-AMS) to facilitate the detection of rBC components and associated coating materials. Incorporation of the light scattering module into the SP-AMS allows the instrument to detect both rBC and NR-PM on a single particle basis; however, this technique has not yet been applied to the characterization of the mixing state of ambient particles.

The primary objective of this study is to demonstrate the capability of the SP-AMS equipped with the light scattering module (LS-SP-AMS) to investigate the mixing state

Single particle
characterization

A. K. Y. Lee et al.

Title Page

Abstract

Introduction

Conclusions

References

Tables

Figures

◀

▶

◀

▶

Back

Close

Full Screen / Esc

Printer-friendly Version

Interactive Discussion



of ambient rBC-containing particles. Clustering analysis using the k -means algorithm, which has been widely applied to analyze ATOFMS data, is performed to classify mass spectra from ambient single particles. The clustering results are used to evaluate the mixing state of ambient particles measured in downtown Toronto and to validate the interpretation of factors from PMF analysis of simultaneously obtained SP-AMS ensemble measurements.

2 Experiment

2.1 Soot particle aerosol mass spectrometer

An Aerodyne soot particle aerosol mass spectrometer (SP-AMS) was deployed to quantify both NR-PM (i.e., ammonium, nitrate, sulfate and organic) and rBC at the St. George campus of University of Toronto in downtown Toronto during 18–22 September 2012. The working principle of the SP-AMS has been reported in detail previously (Onasch et al., 2012). In brief, the SP-AMS is a standard HR-ToF-AMS coupled with a diode-pumped Nd:YAG intracavity 1064 nm infrared (IR) laser vaporizer (see Fig. 1). In the standard AMS configuration, a resistively heated tungsten vaporizer is operated at $\sim 600^\circ\text{C}$ to vaporize the NR-PM (Canagaratna et al., 2007). The addition of the laser vaporizer expands the utility of the standard AMS to vaporize near-IR light absorbing aerosol particles, especially rBC. The rBC-containing particles are heated by absorbing IR energy to $\sim 4000\text{ K}$ to facilitate their vaporization. The resulting gas phase species from either the laser or tungsten vaporizer are ionized with electron impact (EI) ionization (70 eV). The ions are then detected by a high-resolution time-of-flight mass spectrometer operated in V-mode.

The IR laser vaporizer mode was switched on and off during data acquisition. When the IR laser was off, the SP-AMS was operated as a standard HR-ToF-AMS for measuring NR-PM as described above, whereas the instrument operated in the IR laser on mode detects both rBC and NR-PM. An aerodynamically focused particle beam

Single particle characterization

A. K. Y. Lee et al.

Title Page

Abstract

Introduction

Conclusions

References

Tables

Figures



Back

Close

Full Screen / Esc

Printer-friendly Version

Interactive Discussion



overlaps perpendicularly with the IR laser vaporizer before it hits the tungsten vaporizer, and hence the NR-PM that is internally mixed with rBC core is vaporized by the IR laser (Onasch et al., 2012). In addition to the ensemble measurements (i.e., mass spectrum (MS) and particle time-of-flight (PToF) modes to measure bulk and size-resolved chemical composition, respectively), a light scattering module was integrated into the SP-AMS for detecting single particle mass spectra (LSSP mode, see Sect. 2.2 for details). The single particle data are particularly useful for determining the mixing state of ambient aerosol particles. Information on menu switching (90 s each) in the SP-AMS is shown in Table 1.

Ammonium nitrate (NH_4NO_3) particles generated by a constant output atomizer (TSI Inc., Model 3076) were dried using a diffusion dryer, and subsequently size selected at 300 nm using a differential mobility analyzer (DMA, TSI Inc., Model 3081) for determining the ionization efficiency of the SP-AMS when operated in the IR laser off mode. Similarly, a water suspension of Regal Black (Regal 400R Pigment, Cabot Corp.) was atomized to generate standard BC particles. Dried 300 nm Regal Black particles were used to determine the mass-based ionization efficiency of rBC, for calculation of the ionization efficiency relative to nitrate (RIE_{rBC}) (Onasch et al., 2012; Willis et al., 2014). The ensemble data were processed using the AMS data analysis software (Squirrel, version 1.51H for unit mass resolution data and Pika, version 1.10H for high resolution peak fitting) with the corrected air fragment column of the standard fragmentation table (Allan et al., 2004; DeCarlo et al., 2006). Signals of rBC were quantified by the sum of carbon ion clusters (C_x^+) using high resolution mass spectral data up to m/z 120. The product of density and shape factor, derived from the ratio of the vacuum aerodynamic diameter (d_{va}) measured by the PToF mode of the SP-AMS to the mobility diameter (d_{m}) determined by the DMA (DeCarlo et al., 2004) (i.e., $d_{\text{va}} = \rho \times S \times d_{\text{m}} / \rho_0$, where ρ and S are the density and Jayne shape factor of Regal Black particles, respectively, and ρ_0 is the unit density), of the dried 300 nm Regal Black particles is $\sim 0.8 \text{ g cm}^{-3}$. The RIE_{rBC} determined in this study was 0.4, and the default RIE values of nitrate (1.1), sulfate (1.2), organics (1.4) and ammonium (4) were used (Jimenez et al., 2003).

The average C_1^+ to C_3^+ ratio (0.61) obtained from Regal Black was used to correct the interference in C_1^+ from the non-refractory organics in ambient aerosol. The size distribution of rBC was calculated by adding an rBC column (C_1^+ to C_5^+ fragments) to the fragmentation table in Squirrel as shown Table S1 in the Supplement.

2.2 Light scattering module for single particle detection

The design and working principles of the light scattering module have been previously described in detail (Cross et al., 2009; Freutel et al., 2013; Liu et al., 2013). Briefly, the light scattering module consists of a 50 mW diode pumped 405 nm continuous wave laser (CrystaLaser, LC BCL-050-405) that overlaps perpendicularly with the particle beam in the middle of a particle-sizing chamber (~ 0.265 m from the chopper) as shown in Fig. 1. Note that the laser beam is not focused and diverges in order to ensure a complete overlap between the laser and particle beams (Cross et al., 2007). Scattered light from sampled particles is collected using an ellipsoidal mirror and detected with a photomultiplier tube (PMT). A light scattering signal can be obtained if a sampled particle is larger than the optical detection limit. The 50 % cut-off mobility diameter (d_m) of our light scattering module determined using dry NH_4NO_3 particles is ~ 250 nm, which is approximately equal to a vacuum aerodynamic diameter (d_{va}) of ~ 340 nm (the density and shape factor of NH_4NO_3 particles are 1.72 g cm^{-3} and 0.8, respectively). Note that some ambient particles with lower particle densities may have a lower cut-off diameter than that determined for the dried NH_4NO_3 particles. For example, a hydrocarbon oil droplet (i.e., shape factor ~ 1 and density $\sim 1 \text{ g cm}^{-3}$) likely has a light scattering cut-off d_{va} from 225 to 250 nm.

2.3 Single particle categorization

Once a light scattering signal is detected, the computer is triggered to save the corresponding mass spectrum from that individual particle. The PToF data (i.e., particle flight time between the running chopper and the light scattering laser or laser/tungsten

Single particle characterization

A. K. Y. Lee et al.

Title Page

Abstract

Introduction

Conclusions

References

Tables

Figures



Back

Close

Full Screen / Esc

Printer-friendly Version

Interactive Discussion



Single particle
characterization

A. K. Y. Lee et al.

Title Page

Abstract

Introduction

Conclusions

References

Tables

Figures



Back

Close

Full Screen / Esc

Printer-friendly Version

Interactive Discussion



vaporizer) can be used to calculate the d_{va} of all recorded single particles so that a size distribution of the entire single particle dataset can be obtained. Light scattering and single particle mass spectral measurements were processed using the AMS light scattering data processing software (Sparrow, 1.04E), which is designed for analyzing mass spectra with unit mass resolution (UMR) only. The weak scattering trigger events (i.e., a total scattering signal less than 0.2 or a signal-to-noise ratio less than 5) were classified as “rotten” LS events, and they were not included in the subsequent particle categorization. For particles that gave a strong scattering signal and a total number of ions ≥ 6 in their mass spectra, they were either categorized as “prompt”, “early” or “delayed” particle types based on their PToF information. Specifically, when the PToF recorded by the light scattering signal (LS_{PToF}) could accurately predict the particle arrival time to the mass spectrometer (MS_{PToF}) the particle is categorized as prompt. The Gaussian fit of the difference between LS_{PToF} and MS_{PToF} (i.e., $LS_{PToF} - MS_{PToF}$) was used to define the prompt particle boundaries (i.e., particles falling outside the Gaussian fit boundaries (3σ) were either assigned as “early” or “delayed” particle types).

The calculation of total ion signals of an individual particle was modified in the standard software. Instead of using the default output from the fragmentation table, the total number of ions is the sum of all ion signals except m/z 14 (N^+), 15 (NH^+), 16 (NH_2^+), 17 (NH_3^+), 18 (H_2O^+), 28 (N_2^+), 32 (O_2^+) and 39 (K^+) either due to the strong interferences from air and instrument background or the noisy baseline of ammonium fragment ions. Multiple scattering signals observed in a trigger event and weak total ion signal (< 6 ions) were recognized as “coincidence” and “null” particle types, respectively. A summary of the particle categorization in different SP-AMS modes is presented in Table 1. The size distributions of prompt particles in terms of light scattering signal intensity and total number of ions in an individual particle spectrum are shown in Fig. S1 in the Supplement. It is apparent that the particle categorization procedure effectively separates the prompt particles from the full single particle dataset.

2.4 Clustering analysis for single particle data

Clustering analysis was performed to investigate the mixing state of prompt particles based on the k -means algorithm in IGOR Pro (WaveMetrics Inc., version 6.2.2.2). K -means clustering analysis has been extensively applied to analyze single particle data measured from the TSI aerosol time-of-flight mass spectrometer (ATOFMS) (Friedman et al., 2009; Giorio et al., 2012; Gross et al., 2010; Healy et al., 2010, 2013; Pagels et al., 2013) and more recently a standard HR-ToF-AMS with a light scattering module (Liu et al., 2013). Similar to the calculation of total ion signals in a single particle, m/z 14, 15, 16, 17, 18, 28, 32 and 39 were excluded in the clustering analysis. All single particle mass spectra were normalized by their total ion signal, and solutions with up to 25 clusters were tested. Euclidian distance (the square root of the sum of the squares of the differences between corresponding values) was used to evaluate the total distance between the cluster centers and each single particle. In general, increasing the number of clusters can better represent the dataset mathematically (i.e., reduce the total distance) as shown in Fig. S2 in the Supplement. However, a very large number of clusters compromises the physical meaning of each cluster.

A Clustering Analysis Panel (CAP) recently developed by our group was used to perform the k -means clustering analysis. The following information for each cluster can be generated: (1) number of particles, (2) normalized ion-weighted average unit mass resolution mass spectrum, (3) normalized histogram of the frequency of occurrence for each m/z ion signal for each single particle, and (4) average, time- and size-resolved chemical composition (nitrate, sulfate, organics and rBC) in terms of ion counts. Note that the CAP can also combine a few clusters to a single cluster if they have similar mass spectral features and size distributions, whereas other clusters remain unchanged. To avoid generating negative ion signals from the default fragmentation table in Sparrow, a simplified version of the fragmentation table was applied for calculating the chemical composition as shown in Table S2 of the Supplement.

Single particle characterization

A. K. Y. Lee et al.

Title Page

Abstract

Introduction

Conclusions

References

Tables

Figures



Back

Close

Full Screen / Esc

Printer-friendly Version

Interactive Discussion



3 Results and discussion

3.1 Overview of ensemble measurements

Figure 2a shows the time series of NR-PM, measured by the IR laser off mode (i.e., the standard HR-ToF-AMS configuration), and rBC, measured in IR laser on mode, of the whole sampling period in downtown Toronto. In general, organics dominated the particulate mass, whereas rBC contributed 5–8 % of the average particle mass, assuming the collection efficiency (CE) for ambient rBC varies between 0.6 and 1 (i.e., CE range for bare and heavily coated Regal Black particles, respectively) (Willis et al., 2014) and the CE for all NR-PM evaporated from tungsten vaporizer is equal to 1. Willis et al. (2014) reported that the particle beam width (i.e., a primary parameter that governs the CE of rBC in SP-AMS) of ambient rBC particles measured at the same location of downtown Toronto is similar to that of heavily coated Regal Black particles generated in the laboratory. The total particle mass loading measured by the SP-AMS is similar to that inferred from a simultaneous measurement using a Scanning Mobility Particle Sizer (SMPS, TSI Inc.), suggesting that the assumed CE for all NR-PM and rBC are reasonable. The average mass spectrum of rBC was dominated by carbon ion clusters from C_1^+ to C_5^+ (~ 95 %), with the strongest rBC signal at C_3^+ (Fig. 2b). These spectral characteristics are similar to previous SP-AMS measurements (Massoli et al., 2012; Onasch et al., 2012) and the calibration standard used in the current study (Regal Black, see insert of Fig. 2b). Fullerene type rBC spectral features (i.e., C_x^+ fragments with carbon number > 32) were not clearly observed. Onasch et al. (2012) observed carbon cluster ions up to C_{82}^+ in laboratory generated ethylene flame soot particles and detected C_{32}^+ to C_{70}^+ that accounted for about 4 % of the total rBC signals at an urban roadside environment.

Figure 2c displays the average size distributions (PToF d_{va}) of NR-PM and rBC. Secondary inorganic species, nitrate and sulfate, peaked at ~ 300–400 nm with much less contribution to the mass of smaller size particles. In contrast, the rBC signals peaked at ~ 100 nm. Since ambient BC is only emitted from primary sources, this suggests that

Title Page

Abstract

Introduction

Conclusions

References

Tables

Figures



Back

Close

Full Screen / Esc

Printer-friendly Version

Interactive Discussion



Single particle
characterization

A. K. Y. Lee et al.

Title Page

Abstract

Introduction

Conclusions

References

Tables

Figures



Back

Close

Full Screen / Esc

Printer-friendly Version

Interactive Discussion



a significant portion of sampled rBC was freshly emitted or only slightly aged particles. Organic species covered a wide range of particle sizes, and thus they may be internally mixed with rBC and inorganic species. The organic fragment at m/z 44 (CO_2^+) that can be used as a tracer of oxygenated SOA (e.g., organic acids) exhibited a bimodal distribution with the larger particle mode comparable to sulfate and nitrate (Fig. 2c). Nevertheless, additional information such as single particle characterization is required to confirm the mixing state of ambient particles. The average O/C and H/C ratios of total organics obtained from elemental analysis of high resolution mass spectral data are 0.28 (ranged from 0.05 to 0.57) and 1.65 (ranged from 1.47 to 1.82), respectively (see the Van Krevelen diagram in Fig. S3 in the Supplement). The relatively low degree of oxygenated organic aerosol indicates that the sampling site was strongly influenced by local anthropogenic sources, such as vehicle and cooking related emissions.

3.2 PMF analysis of ensemble measurements

Positive matrix factorization (PMF) has been widely applied to analyze ambient AMS datasets to identify the potential sources of organic aerosol (Ulbrich et al., 2009; Zhang et al., 2011). PMF analysis separates the total organics measured in this study (Fig. 3a–c) into factors that have been commonly observed in AMS measurements: hydrocarbon-like organic aerosol (HOA), cooking emission organic aerosol (COA), and oxygenated organic aerosol (OOA) (Zhang et al., 2011 and references therein). In brief, the HOA spectrum exhibits fragmentation patterns associated with hydrocarbon structures (e.g., m/z 57 (C_4H_9^+), 69 (C_5H_9^+), etc.), and is comparable to those of gasoline/diesel vehicle exhaust and lubricating oil (Canagaratna et al., 2004; Massoli et al., 2012; Mohr et al., 2009). The COA and HOA spectra are similar to each other; however, the COA factor tends to have a higher ratio of m/z 55 to 57 (Allan et al., 2010; Mohr et al., 2012, 2009). Lastly, the OOA spectrum is composed of a relatively high fraction of m/z 44 (CO_2^+), indicating that the OOA materials have a larger photochemical age (Jimenez et al., 2009; Ng et al., 2010). The O/C and H/C ratios of the laser

off mode PMF factors and their coordinates in the Van Krevelen diagram are shown in Figs. 3a–c and S3 in the Supplement, respectively.

Figure 4 shows the time series of the three-factor PMF solution obtained with the IR laser off. Significant contributions of HOA and COA to the total organic mass (average \pm standard deviation = 52 % \pm 20 %) indicate that the sampling site was strongly influenced by anthropogenic emissions (Fig. S4 in the Supplement). In particular, the temporal variations in rBC and the laser off HOA factor showed a significant correlation (Fig. 4a), demonstrating that the HOA was primarily emitted from combustion sources such as engine exhaust. The substantial COA mass loading is consistent with the fact that many catering facilities are close to the sampling site (Fig. 4b). The strong diurnal cycle of the COA factor was likely due to the active cooking activities from noon to night every day. The OOA factor represents the ambient level of oxygenated organic aerosol that originated from secondary sources and/or was produced by photochemical aging (e.g., transported/regional emissions from outside the city) (Fig. 4c). Similar PMF results were obtained for the IR laser on measurements (excluding rBC signals in the PMF analysis) and are shown in Figs. S5 and S6 in the Supplement. Including the rBC signals only slightly modified the PMF results of the laser on measurements as displayed in Figs. 3d–f and S5 in the Supplement. Based on the PMF analysis, the rBC associated with HOA, COA and OOA accounted for about 51 % (\pm 20 %), 9 % (\pm 11 %) and 40 % (\pm 18 %), respectively, of the total rBC mass loading on average (\pm standard deviation). The temporal variations of rBC mass fractions contributed from each factor are shown in Fig. 3g.

3.3 Comparison of laser on and off ensemble measurements

The IR laser on mode exhibited a higher sensitivity to all NR-PM components than the IR laser off mode by \sim 10–20 %, depending on the chemical species (Fig. S7 in the Supplement). This may be due to different CE issues for the two vaporizers (i.e., incomplete particle-laser beam overlap for laser vaporizer (Willis et al., 2014) and particle bounce issues for tungsten vaporizers (Matthew et al., 2008)). For example, the

Single particle characterization

A. K. Y. Lee et al.

Title Page

Abstract

Introduction

Conclusions

References

Tables

Figures



Back

Close

Full Screen / Esc

Printer-friendly Version

Interactive Discussion



Single particle
characterization

A. K. Y. Lee et al.

Title Page

Abstract

Introduction

Conclusions

References

Tables

Figures



Back

Close

Full Screen / Esc

Printer-friendly Version

Interactive Discussion



instrument operated in the laser off mode might have a lower CE for rBC-containing particles due to particles bouncing off the tungsten vaporizer, an effect which would depend on the phase of the particles. In particular, it is well known that solid/semi-solid particles have a more pronounced bouncing effect than liquid particles (Docherty et al., 2013; Matthew et al., 2008). Furthermore, particle vaporization by the IR laser and the tungsten vaporizer do not occur at the same location inside the ion chamber, possibly resulting in different ionization rates and ion transmission efficiencies (i.e., from the ion chamber to the ion focusing optics) between the two operational modes.

Although the main driver of the observed sensitivity enhancement remains unclear, a larger difference between the two modes would imply that a higher mass fraction of a particular aerosol component coexists with rBC, because rBC-containing ambient particles are evaporated by the IR laser before they can reach the tungsten surface. Compared to the standard AMS measurements, in the laser on mode the HOA, COA and OOA mass loadings are higher by about 40 %, 10 %, and 23 %, respectively (Fig. S8a–c in the Supplement). Figure S8d explicitly demonstrates that the percentage difference of each PMF factor between the laser on and off operational modes is positively correlated with the mass fraction of rBC signal in each factor (mass fraction of rBC in laser on HOA = 0.15, COA = 0.02, and OOA = 0.06). This is indirect evidence that a larger fraction of HOA material was internally mixed with rBC compared to the COA and OOA components. For inorganic species, it is also possible that some refractory nitrate and sulfate (e.g., KNO_3 and Na_2SO_4) and/or acidic materials (e.g., H_2SO_4) coexisted with rBC because the enhancement of NH_4^+ mass between the two operational modes is smaller than those observed in the case of NO_3^- and SO_4^{2-} (Fig. S7 in the Supplement).

3.4 Overview of single particle dataset

The single particle statistics of the LSSP measurement are summarized in Table 1. The IR laser on and off modes had 113 120 and 112 441 total light scattering (LS) trigger events, respectively, and 75 % of them were recognized as particle LS trigger events.

Single particle
characterization

A. K. Y. Lee et al.

Title Page

Abstract

Introduction

Conclusions

References

Tables

Figures



Back

Close

Full Screen / Esc

Printer-friendly Version

Interactive Discussion



Approximately 41 % (35 001) and 34 % (28 322) of the particle LS trigger events were categorized as prompt particles in the laser on and off modes, respectively. Figure 5 shows the prompt single particle results for laser on and off modes, and the difference, as a function of the measured particle sizes (d_{va} , nm). A higher fraction of prompt particles observed in the IR laser on mode could be due to (1) the extra ions generated from rBC, (2) the different CE for laser and tungsten vaporizers, and (3) a higher mass spectral sensitivity in the laser on mode as described in Sect. 3.3. Cross et al. (2009) and Liu et al. (2012) reported that null particles accounted for $\sim 50\%$ of the particle LS trigger events, which is somewhat lower than those determined in this study (Table 1). This may arise from the fact that all ammonium fragments (m/z 14, 15, 16) were excluded in our calculation of total ion signals in the particle categorization procedure. It is also worth noting that Cross et al. (2009) deployed a more sensitive compact ToF-AMS (CToF-AMS) in their measurements, and our instrument likely had a more sensitive light scattering detection system (i.e. better laser alignment) than that used by Liu et al. (2012).

Figure 6 shows some representative examples of single particle mass spectra of rBC-containing particles. Using the ensemble spectrum of rBC as a reference (Fig. 2c), it is clear that ambient rBC can exist as nearly externally mixed (Fig. 6a) or can be associated with various types of coating materials such as HOA (Fig. 6b), OOA and inorganics (Fig. 6c). Figure 7 shows the chemically speciated size distributions of all prompt particles. Even though a significant portion of small particles cannot be detected in the LSSP measurements, the single particle size distributions measured by the laser on and off modes are generally consistent with the ensemble PToF data (Fig. 2c). A light scattering cut-off d_{va} of ambient nitrate and sulfate match well with that calibrated by the dried NH_4NO_3 particles, whereas ambient organic particles that are mainly composed of HOA and COA materials (see Sect. 3.5) have a cut-off d_{va} similar to that estimated for spherical hydrocarbon oil droplets (~ 250 nm, the purple dashed line in Figs. 5 and 7). Furthermore, the LSSP mode can detect rBC-containing particles and the associated coating materials down to ~ 100 nm d_{va} . This is because

Single particle
characterization

A. K. Y. Lee et al.

Title Page

Abstract

Introduction

Conclusions

References

Tables

Figures



Back

Close

Full Screen / Esc

Printer-friendly Version

Interactive Discussion



ambient BC/soot agglomerates can have low effective particle densities due to their fractal morphologies (China et al., 2013, 2014; Slowik et al., 2004). In other words, the ambient BC particles that have small d_{va} can be physically large enough to be detected by the light scattering module (i.e., $d_{va} = \rho \times S \times d_m / \rho_0$, where ρ , S and d_m are particle density, Jayne shape factor and mobility diameter, respectively, and ρ_0 is the unit density) and can produce sufficient signal for mass spectrometric detection.

The differences in overall and chemically speciated size distribution of ion signals between the laser on and off modes are shown in Figs. 5 and 7c, respectively. Accumulation mode particles peaked at ~ 400 nm d_{va} (mainly composed of secondary aerosol components such as nitrate, sulfate and oxygenated organic species) and exhibited the largest differences between the two operational modes. Organics with mid-range d_{va} (i.e., peak at ~ 300 nm) show a relatively small difference compared to accumulation mode organics, suggesting that those organic particles have similar CE between the two operational modes and their ion signals are likely less sensitive to the types of particle vaporization (i.e., no bouncing on tungsten vaporizer (CE = 1) and no rBC core). Note that those mid-range d_{va} organic particles are likely dominated by HOA and COA materials (see Sect. 3.5). Similar observations are also obtained from particle number size distributions as shown in Fig. S9a in the Supplement. The laser on-to-laser off ratios in terms of total ion signals and particle number are biased higher in the large and small particle size ranges. The former is suggestive of potential bounce effects on the tungsten vaporizer, but not the laser vaporizer; the latter, for particles smaller than 200 nm, is likely due to rBC particles dominating the ion signals (Fig. S9b in the Supplement).

3.5 Clustering analysis of single particle data

The k -means clustering algorithm was used to classify all the prompt particle mass spectra into chemically distinct groups. To demonstrate the capability of the LS-SP-AMS to investigate the mixing state of ambient aerosol particles, the twelve-cluster solution from the laser on mode measurements is presented here. The number of

Single particle
characterization

A. K. Y. Lee et al.

Title Page

Abstract

Introduction

Conclusions

References

Tables

Figures



Back

Close

Full Screen / Esc

Printer-friendly Version

Interactive Discussion



particles and the ion fractions of nitrate, sulfate, organics and rBC in each cluster are shown in Fig. S10 in the Supplement. Increasing the number of clusters up to 25 only gradually reduced the total Euclidian distance between the cluster centers and each single particle mass spectrum (Fig. S2 in the Supplement), and does not generate any new clusters with significant physical meaning. By comparing the mass spectra, time series, and size distributions of the twelve clusters, it is clear that some clusters must be re-combined into a single cluster to provide physically meaningful results. For example, four preliminary clusters obtained from the k -means clustering analysis (cluster #1, 6, 8 and 11 in Fig. S10 in the Supplement) are rich in nitrate signatures with similar temporal variations and/or size distributions (Fig. S11 in the Supplement), and hence they were combined to procedure a single nitrate-rich cluster. Merging preliminary clusters into a single final cluster has been widely applied to clustering analysis of ATOFMS data (e.g., Healy et al., 2013). A tracer for rBC (C_3^+ at m/z 36) is used to examine the mixing state of ambient rBC. The potential isobaric interference from HCl^+ was evaluated based on the clustering analysis of the IR laser off dataset (Table 2, see discussion below). Note that the overall clustering analysis results for NR-PM are quite similar for both the IR laser on and off data sets.

3.5.1 Inorganic clusters

Figure 8 summarizes the unit mass resolution (UMR) spectra, mass spectral histograms and size distributions of the seven final clusters. Figure 8a shows a nitrate-rich cluster that consists of significant ion signals at m/z 30 (NO^+) and m/z 46 (NO_2^+) with comparable intensities, and a sulfate-rich cluster with a mass spectrum dominated by m/z 48 (SO^+), 64 (SO_2^+), 80 (SO_3^+), 81 (HSO_3^+) and 98 ($H_2SO_4^+$). These inorganic clusters have narrow size distributions and peak at ~ 400 nm (Fig. 8p and q), which is consistent with the PToF ensemble data. A significant fraction of the particles in these two clusters are internally mixed with a substantial amount of organic material. The mass spectra of these organics are similar to the OOA cluster 1 identified in this work (i.e., strong signals at m/z 29 and 43, Fig. 8f). In particular, approximately 60–70 % of

the nitrate- and sulfate-rich particles exhibit organic signal at m/z 43 (Fig. 8h and i). Furthermore, the tracer of rBC (C_3^+ at m/z 36) indicates that rBC has only a minor contribution to the nitrate- and sulfate-rich particles (i.e., a similar percentage of particles contributed to m/z 36 between laser on and off modes ($< 2\%$) in these clusters) as shown in Table 2.

3.5.2 HOA and rBC clusters

A cluster with mass spectral fragmentation patterns of hydrocarbons (i.e. $C_xH_y^+$ ions) is assigned as a HOA cluster (Fig. 8c). It is important to point out that most of the HOA-rich particles are largely externally mixed with inorganic species (Fig. 8c and j). Only 6.4% of the HOA-rich particles were composed of a detectable signal at m/z 36 that originates from rBC (Table 2) and the mass contribution of rBC to this cluster was about 3% on average ($RIE_{org} = 1.4$ and $RIE_{rBC} = 0.4$). Instead, the clustering analysis yields a separate rBC cluster without substantial organic coating (Fig. 8d). Although the mass fraction contribution of organics to this cluster is only 0.28, ~ 60 – 80% of the particles consist of detectable organic signals at m/z 41, 43, 55, and 57 (Fig. 8k). The rBC-rich cluster has a C_1^+/C_3^+ ratio of about 0.53, which is slightly smaller than the ratio obtained from the calibration standard (Regal Black). The mass spectral character of the organic coating is similar to the spectrum of PMF-HOA in general, but with a slightly higher fraction of m/z 44 and lower fraction of m/z 55 and 57 compared to the HOA cluster (insert of Fig. 8d). We emphasize that while PMF analysis showed that BC and HOA materials likely have the same emission sources, this approach does not provide direct information about the ambient particle mixing state. In contrast, the clustering analysis clearly suggests that two major types of particles contributed to the PMF-HOA factor. The different size distributions of the two clusters also indicate two distinct particle types (Fig. 8r and s).

Single particle characterization

A. K. Y. Lee et al.

Title Page

Abstract

Introduction

Conclusions

References

Tables

Figures

◀

▶

◀

▶

Back

Close

Full Screen / Esc

Printer-friendly Version

Interactive Discussion



3.5.3 COA and OOA clusters

The mass spectrum of a COA cluster is shown in Fig. 8e. The COA cluster covers a range of particles with d_{va} peaking at ~ 300 nm (Fig. 8t). Similar to the PMF-COA factor, the COA cluster is dominated by fragments at m/z 41 and m/z 55 with a relatively high m/z 55 to 57 ratio compared to the HOA. Two OOA clusters were also identified (Fig. 8f and g). These clusters likely represent aged organic aerosol components because a large fraction of the particles ($> 50\%$) are associated with secondary nitrate and sulfate. While OOA cluster 1 represents the less oxygenated organics (i.e., strong signal from less oxygenated fragments such as CHO^+ at m/z 29 and $\text{C}_2\text{H}_3\text{O}^+$ at m/z 43), OOA cluster 2 has the distinct spectral feature of highly oxygenated organics produced via photochemical aging (i.e., intense signal at m/z 44 (CO_2^+) from organic acids). Both clusters have size distributions similar to the inorganic clusters. The major exception is that the OOA cluster 1 has another peak with a smaller mean particle diameter, suggesting that this cluster may consist of ambient particles with a different degree of aging (e.g., fewer condensed materials such as inorganic species on the smaller particles). The majority of the particles in the COA and OOA clusters (96–97 %) were not associated with rBC signals (Table 2).

3.6 Low to mid-range d_{va} , organic-rich particles

The results provide a valuable, new perspective into the chemical composition and potential sources for low to mid-range d_{va} , organic-rich particles (i.e., dominated by particles in the HOA and COA clusters) using both ensemble and single particle techniques. Specifically, we made two sets of observations: (a) SP-AMS ensemble data suggest that HOA and rBC were highly correlated in several ways: (1) time traces in Fig. 4a, (2) PToF size distributions in Fig. 2c, and (3) laser on-to-laser off ratios for PMF factors in Figs. S7 and S8 in the Supplement; and (b) LS-SP-AMS single particle results suggest that HOA- and COA-rich particles were nearly externally mixed with rBC. The strong correlation between HOA and rBC has, for the most part, been noted

Single particle characterization

A. K. Y. Lee et al.

[Title Page](#)[Abstract](#)[Introduction](#)[Conclusions](#)[References](#)[Tables](#)[Figures](#)[⏪](#)[⏩](#)[◀](#)[▶](#)[Back](#)[Close](#)[Full Screen / Esc](#)[Printer-friendly Version](#)[Interactive Discussion](#)

Single particle
characterization

A. K. Y. Lee et al.

Title Page

Abstract

Introduction

Conclusions

References

Tables

Figures



Back

Close

Full Screen / Esc

Printer-friendly Version

Interactive Discussion



previously (Zhang et al., 2011 and references therein). The new observations obtained with the LS-SP-AMS single particle data and k -means clustering analysis suggest that the low to mid-range d_{va} , organic-rich particles in a typical urban environment largely arise from low density organic materials, such as nearly pure HOA and COA particles (> 95 wt% of organics) emitted from primary sources (e.g., vehicle exhaust and cooking emissions).

Even though the HOA-rich and rBC-rich particles exhibit near external mixing, we do note that HOA materials are nevertheless still more closely associated with rBC than are other particle constituents. As noted above, the laser on-to-laser off ratio increases by organic PMF factor in the following manner: HOA > OOA > COA (Fig. S8 in the Supplement). This trend correlates well with the observed ensemble rBC mass fractions for each PMF factor. Hence, the difference between the PMF-HOA mass loadings from the laser on and off modes suggests that HOA materials were more associated with rBC-containing particles than were OOA and COA. Furthermore, the thin HOA coating on rBC-rich particles alone is likely insufficient to explain the PMF-HOA difference between laser on and off modes, at least for the current single particle size range. This suggests that the HOA-rich particles were likely associated with small rBC cores.

Quantitatively, the single particle data analysis demonstrates that: (1) a significant portion of HOA- and COA-rich particles (> 90 %) with particle d_{va} larger than ~ 200 nm did not contain a detectable amount of rBC, i.e., the particles can be thought of containing a small rBC core with a thick HOA coating (with a mass contribution of rBC to the HOA- and COA-rich cluster about 3 % on average), and (2) the rBC-rich particles were mixed with ~ 28 wt% HOA-like material on average, i.e., a thinly HOA coated rBC particle. rBC was mixed to a minor extent with other inorganic and organic materials. The total organic-to-rBC ratios are relatively constant across the size range of the rBC-rich cluster. However, whether this fact allows us to extend our mixing state conclusions to particles that are smaller than the nominal detection limit of the light scattering module is unknown.

Single particle
characterization

A. K. Y. Lee et al.

Title Page

Abstract

Introduction

Conclusions

References

Tables

Figures



Back

Close

Full Screen / Esc

Printer-friendly Version

Interactive Discussion



The number fraction of rBC-containing particles to total prompt particles determined in the current study is about 7–11 % using m/z 36 as an rBC tracer and considering the potential interference from HCl^+ (Table 2). Willis et al. (2014) showed that the SP-AMS could measure rBC mass fractions down to at least 5 % by mass for laboratory-generated particle ensembles. The current data suggest that per particle rBC mass fractions for many of the HOA- and COA-rich single particles are less than 5 % (Table 2). We cannot rule out that the SP-AMS is missing ion signals from small rBC cores in these particle types. The fact that the RIE_{rBC} (usually from 0.2 to 0.4) is smaller than the RIE of other major NR-PM species indicates that that we are getting fewer ion signals per mass from rBC compared to other NR-PM components, making it harder to determine if rBC is in any given particle. Therefore, the single particle mixing state measurements here may under represent rBC-containing particle number (and mass) not only for low to mid-range d_{va} , organic-rich particles but also for all identified clusters.

3.7 Comparison of clustering observations with PMF factors

In addition to the mass spectral comparison provided in the previous section, Fig. 4 displays a comparison between the time series of organic clusters (HOA, COA, and OOA clusters, in ion signal) and PMF factors (in mass loadings). The total signals of the OOA cluster shown in Fig. 4c were determined by the sum of organic signals from the nitrate, sulphate, OOA 1 and OOA 2 clusters as they all contain oxygenated organic aerosol materials. The COA cluster completely captures the diurnal cycle of the PMF-COA (Fig. 4b), and the PMF-OOA agrees well with the OOA clusters (Fig. 4c). The PMF-HOA factor exhibited three major peaks during the sampling period indicated by red dashed rectangles in Fig. 4a. However, the HOA cluster only captures the first two periods and not the last one. It is possible that most of the HOA material in this final period was associated with extremely small particles, which could not be detected by the light scattering module. The HOA cluster organic signals displayed in Fig. 4a are not significantly altered by the addition of organic signals from the rBC cluster. Overall, the temporal variations of these organic clusters and PMF factors correlate very well

indicating that this single particle approach is able to largely capture the variability in the major aerosol components.

4 Summary and concluding remarks

This work is the first report of single particle characterization of rBC particles with the LS-SP-AMS, and successfully demonstrates the application of this instrument to determine the mixing state of ambient rBC. PMF analysis of ensemble data is a standard approach used to investigate the sources of ambient organic aerosol. Noting that the single particle data are direct measurements of aerosol composition whereas PMF analysis is a statistical tool, a major result from this paper is the temporal and compositional agreement between *k*-means single particle clusters and the PMF factors, which validate the PMF result and their relation to particulate matter sources.

Additional information regarding the mixing state of ambient particles and their size distributions (down to the detection limit of the light scattering module) are important for improving our understanding of the environmental impacts of atmospheric aerosol particles. While Liu et al. (2013) first applied the *k*-mean clustering algorithm to LS-ToF-AMS data, this work successfully extends the application of the *k*-means clustering approach to analyze LS-SP-AMS data to evaluate the mixing state of ambient rBC particles and other non-refractory aerosol components. The approach presented here can be applied to assess the magnitude of the contributions of different sources when performing source-receptor analysis.

While it is recognized that HOA factors, identified by PMF analysis of standard HR-ToF-AMS data, and rBC originate from combustion sources, the mixing states of these primary aerosol species cannot be easily characterized in this manner. Within the constraints of the instrumentation that may under represent the number of rBC-containing particles (see Sects. 3.3 and 3.6), the single particle data analysis demonstrates quantitatively that there were two types of particles associated with HOA materials: (1) HOA-rich particles associated with ~ 3 wt% of rBC (i.e., a small rBC core with thick

Single particle characterization

A. K. Y. Lee et al.

Title Page

Abstract

Introduction

Conclusions

References

Tables

Figures



Back

Close

Full Screen / Esc

Printer-friendly Version

Interactive Discussion



Single particle
characterization

A. K. Y. Lee et al.

Title Page

Abstract

Introduction

Conclusions

References

Tables

Figures



Back

Close

Full Screen / Esc

Printer-friendly Version

Interactive Discussion



HOA coating), and (2) rBC-rich particles mixed with ~ 28 wt% HOA-like material on average (i.e., a thinly HOA coated rBC particle). Other inorganic and organic materials were mixed to a lesser extent with rBC. The single particle data also provide insight to the sources of low to mid-range d_{va} organics in a typical urban environment. According to our clustering analysis, those organics are mainly composed of HOA- and COA-rich particles emitted from primary sources such as vehicle exhaust and kitchen emissions instead of processed particles associated with condensed secondary materials.

During our study, most of the BC was likely freshly emitted from nearby vehicle exhaust and therefore we did not observe significant mixing. Further deployment of the LS-SP-AMS in remote environments will provide insight into the mixing state of aged ambient BC. Freutel et al. (2013) recently developed a new particle categorization algorithm based on reference spectra comparison, which is potentially useful to identify unknown rBC particle types from LS-SP-AMS measurements.

**The Supplement related to this article is available online at
doi:10.5194/acpd-14-15323-2014-supplement.**

Acknowledgements. This work was financially supported by Natural Sciences and Engineering Research Council (NSERC) of Canada, the Canada Foundation for Innovation and the Marie Curie Action FP7-PEOPLE-IOF-2011 (Project: CHEMBC, No. 299755).

References

- Allan, J., Delia, A., Coe, H., Bower, K., Alfarra, M., Jimenez, J., Middlebrook, A., Drewnick, F., Onasch, T., Canagaratna, M., Jayne, J., and Worsnop, D.: A generalised method for the extraction of chemically resolved mass spectra from Aerodyne aerosol mass spectrometer data, *J. Aerosol Sci.*, 35, 909–922, 2004.
- Allan, J. D., Williams, P. I., Morgan, W. T., Martin, C. L., Flynn, M. J., Lee, J., Nemitz, E., Phillips, G. J., Gallagher, M. W., and Coe, H.: Contributions from transport, solid fuel burning

Single particle
characterization

A. K. Y. Lee et al.

Title Page

Abstract

Introduction

Conclusions

References

Tables

Figures



Back

Close

Full Screen / Esc

Printer-friendly Version

Interactive Discussion



and cooking to primary organic aerosols in two UK cities, *Atmos. Chem. Phys.*, 10, 647–668, doi:10.5194/acp-10-647-2010, 2010.

Baumgardner, D., Kok, G., and Raga, G.: Warming of the Arctic lower stratosphere by light absorbing particles, *Geophys. Res. Lett.*, 31, L06117, doi:10.1029/2003GL018883, 2004.

5 Bond, T. C., Doherty, S. J., Fahey, D. W., Forster, P. M., Berntsen, T., DeAngelo, B. J., Flanner, M. G., Ghan, S., Kaercher, B., Koch, D., Kinne, S., Kondo, Y., Quinn, P. K., Sarofim, M. C., Schultz, M. G., Schulz, M., Venkataraman, C., Zhang, H., Zhang, S., Bellouin, N., Guttikunda, S. K., Hopke, P. K., Jacobson, M. Z., Kaiser, J. W., Klimont, Z., Lohmann, U., Schwarz, J. P., Shindell, D., Storelvmo, T., Warren, S. G., and Zender, C. S.: Bounding the
10 role of black carbon in the climate system: a scientific assessment, *J. Geophys. Res.-Atmos.*, 118, 5380–5552, 2013.

Canagaratna, M. R., Jayne, J. T., Ghertner, D. A., Herndon, S., Shi, Q., Jimenez, J. L., Silva, P. J., Williams, P., Lanni, T., Drewnick, F., Demerjian, K. L., Kolb, C. E., and Worsnop, D. R.: Chase studies of particulate emissions from in-use New York City vehicles,
15 *Aerosol Sci. Tech.*, 38, 555–573, 2004.

Canagaratna, M. R., Jayne, J. T., Jimenez, J. L., Allan, J. D., Alfarra, M. R., Zhang, Q., Onasch, T. B., Drewnick, F., Coe, H., Middlebrook, A., Delia, A., Williams, L. R., Trimborn, A. M., Northway, M. J., DeCarlo, P. F., Kolb, C. E., Davidovits, P., and Worsnop, D. R.:
20 Chemical and microphysical characterization of ambient aerosols with the aerodyne aerosol mass spectrometer, *Mass Spectrom. Rev.*, 26, 185–222, 2007.

Cappa, C. D., Onasch, T. B., Massoli, P., Worsnop, D. R., Bates, T. S., Cross, E. S., Davidovits, P., Hakala, J., Hayden, K. L., Jobson, B. T., Kolesar, K. R., Lack, D. A., Lerner, B. M., Li, S., Mellon, D., Nuaaman, I., Olfert, J. S., Petaja, T., Quinn, P. K., Song, C., Subramanian, R., Williams, E. J., and Zaveri, R. A.: Radiative absorption enhancements due to the
25 mixing state of atmospheric black carbon, *Science*, 337, 1078–1081, 2012.

China, S., Mazzoleni, C., Gorkowski, K., Aiken, A. C., and Dubey, M. K.: Morphology and mixing state of individual freshly emitted wildfire carbonaceous particles, *Nat. Commun.*, 4, 2122, doi:10.1038/ncomms3122, 2013.

China, S., Salvadori, N., and Mazzoleni, C.: Effect of traffic and driving characteristics on morphology of atmospheric soot particles at freeway on-ramps, *Environ. Sci. Technol.*, 48, 3128–
30 3135, 2014.

Cross, E. S., Slowik, J. G., Davidovits, P., Allan, J. D., Worsnop, D. R., Jayne, J. T., Lewis, D. K., Canagaratna, M., and Onasch, T. B.: Laboratory and ambient particle density determinations

Single particle
characterization

A. K. Y. Lee et al.

Title Page

Abstract

Introduction

Conclusions

References

Tables

Figures



Back

Close

Full Screen / Esc

Printer-friendly Version

Interactive Discussion



using light scattering in conjunction with aerosol mass spectrometry, *Aerosol Sci. Tech.*, 41, 343–359, 2007.

Cross, E. S., Onasch, T. B., Canagaratna, M., Jayne, J. T., Kimmel, J., Yu, X.-Y., Alexander, M. L., Worsnop, D. R., and Davidovits, P.: Single particle characterization using a light scattering module coupled to a time-of-flight aerosol mass spectrometer, *Atmos. Chem. Phys.*, 9, 7769–7793, doi:10.5194/acp-9-7769-2009, 2009.

Cross, E. S., Onasch, T. B., Ahern, A., Wrobel, W., Slowik, J. G., Olfert, J., Lack, D. A., Massoli, P., Cappa, C. D., Schwarz, J. P., Spackman, J. R., Fahey, D. W., Sedlacek, A., Trimborn, A., Jayne, J. T., Freedman, A., Williams, L. R., Ng, N. L., Mazzoleni, C., Dubey, M., Brem, B., Kok, G., Subramanian, R., Freitag, S., Clarke, A., Thornhill, D., Marr, L. C., Kolb, C. E., Worsnop, D. R., and Davidovits, P.: Soot Particle Studies Instrument Inter-Comparison Project overview, *Aerosol Sci. Tech.*, 44, 592–611, 2010.

DeCarlo, P. F., Slowik, J. G., Worsnop, D. R., Davidovits, P., and Jimenez, J. L.: Particle morphology and density characterization by combined mobility and aerodynamic diameter measurements, Part 1: theory, *Aerosol Sci. Tech.*, 38, 1185–1205, 2004.

DeCarlo, P. F., Kimmel, J. R., Trimborn, A., Northway, M. J., Jayne, J. T., Aiken, A. C., Gonin, M., Fuhrer, K., Horvath, T., Docherty, K. S., Worsnop, D. R., and Jimenez, J. L.: Field-deployable, high-resolution, time-of-flight aerosol mass spectrometer, *Anal. Chem.*, 78, 8281–8289, 2006.

Drewnick, F., Hings, S. S., DeCarlo, P. F., Jayne, J. T., Gonin, M., Fuhrer, K., Weimer, S., Jimenez, J. L., Demerjian, K. L., Borrmann, S., and Worsnop, D. R.: A new time-of-flight aerosol mass spectrometer (TOF-AMS) – instrument description and first field deployment, *Aerosol Sci. Tech.*, 39, 637–658, 2005.

Docherty, K. S., Jaoui, M., Corse, E., Jimenez, J. L., Offenberg, J. H., Lewandowski, M., and Kleindienst, T. E.: Collection efficiency of the Aerosol Mass Spectrometer for chamber-generated secondary organic aerosols, *Aerosol Sci. Tech.*, 47, 294–309, 2013.

Freutel, F., Drewnick, F., Schneider, J., Klimach, T., and Borrmann, S.: Quantitative single-particle analysis with the Aerodyne aerosol mass spectrometer: development of a new classification algorithm and its application to field data, *Atmos. Meas. Tech.*, 6, 3131–3145, doi:10.5194/amt-6-3131-2013, 2013.

Friedman, B., Herich, H., Kammermann, L., Gross, D. S., Arneith, A., Holst, T., and Cziczo, D. J.: Subarctic atmospheric aerosol composition: 1. Ambient aerosol characterization, *J. Geophys. Res.-Atmos.*, 114, D13203, doi:10.1029/2009JD011772, 2009.

Single particle
characterization

A. K. Y. Lee et al.

Title Page

Abstract

Introduction

Conclusions

References

Tables

Figures



Back

Close

Full Screen / Esc

Printer-friendly Version

Interactive Discussion



Giorio, C., Tapparo, A., Dall'Osto, M., Harrison, R. M., Beddows, D. C. S., Di Marco, C., and Nemitz, E.: Comparison of three techniques for analysis of data from an Aerosol Time-of-Flight Mass Spectrometer, *Atmos. Environ.*, 61, 316–326, 2012.

Gross, D. S., Atlas, R., Rzeszutarski, J., Turetsky, E., Christensen, J., Benzaid, S., Olson, J., Smith, T., Steinberg, L., Sulman, J., Ritz, A., Anderson, B., Nelson, C., Musicant, D. R., Chen, L., Snyder, D. C., and Schauer, J. J.: Environmental chemistry through intelligent atmospheric data analysis, *Environ. Modell. Softw.*, 25, 760–769, 2010.

Healy, R. M., Hellebust, S., Kourtchev, I., Allanic, A., O'Connor, I. P., Bell, J. M., Healy, D. A., Sodeau, J. R., and Wenger, J. C.: Source apportionment of PM_{2.5} in Cork Harbour, Ireland using a combination of single particle mass spectrometry and quantitative semi-continuous measurements, *Atmos. Chem. Phys.*, 10, 9593–9613, doi:10.5194/acp-10-9593-2010, 2010.

Healy, R. M., Sciare, J., Poulain, L., Crippa, M., Wiedensohler, A., Prévôt, A. S. H., Baltensperger, U., Sarda-Estève, R., McGuire, M. L., Jeong, C.-H., McGillicuddy, E., O'Connor, I. P., Sodeau, J. R., Evans, G. J., and Wenger, J. C.: Quantitative determination of carbonaceous particle mixing state in Paris using single-particle mass spectrometer and aerosol mass spectrometer measurements, *Atmos. Chem. Phys.*, 13, 9479–9496, doi:10.5194/acp-13-9479-2013, 2013.

Jacobson, M.: Strong radiative heating due to the mixing state of black carbon in atmospheric aerosols, *Nature*, 409, 695–697, 2001.

Jimenez, J. L., Jayne, J. T., Shi, Q., Kolb, C. E., Worsnop, D. R., Yourshaw, I., Seinfeld, J. H., Flagan, R. C., Zhang, X., Smith, K. A., Morris, J. W., and Davidovits, P.: Ambient aerosol sampling using the Aerodyne Aerosol Mass Spectrometer, *J. Geophys. Res.-Atmos.*, 108, 8425, doi:10.1029/2001JD001213, 2003.

Jimenez, J. L., Canagaratna, M. R., Donahue, N. M., Prevot, A. S. H., Zhang, Q., Kroll, J. H., DeCarlo, P. F., Allan, J. D., Coe, H., Ng, N. L., Aiken, A. C., Docherty, K. S., Ulbrich, I. M., Grieshop, A. P., Robinson, A. L., Duplissy, J., Smith, J. D., Wilson, K. R., Lanz, V. A., Hueglin, C., Sun, Y. L., Tian, J., Laaksonen, A., Raatikainen, T., Rautiainen, J., Vaattovaara, P., Ehn, M., Kulmala, M., Tomlinson, J. M., Collins, D. R., Cubison, M. J., Dunlea, E. J., Huffman, J. A., Onasch, T. B., Alfarra, M. R., Williams, P. I., Bower, K., Kondo, Y., Schneider, J., Drewnick, F., Borrmann, S., Weimer, S., Demerjian, K., Salcedo, D., Cottrell, L., Griffin, R., Takami, A., Miyoshi, T., Hatakeyama, S., Shimono, A., Sun, J. Y., Zhang, Y. M., Dzepina, K., Kimmel, J. R., Sueper, D., Jayne, J. T., Herndon, S. C., Trimborn, A. M.,

Single particle
characterization

A. K. Y. Lee et al.

Title Page

Abstract

Introduction

Conclusions

References

Tables

Figures



Back

Close

Full Screen / Esc

Printer-friendly Version

Interactive Discussion



Williams, L. R., Wood, E. C., Middlebrook, A. M., Kolb, C. E., Baltensperger, U., and Worsnop, D. R.: Evolution of organic aerosols in the atmosphere, *Science*, 326, 1525–1529, 2009.

Lack, D. A., Langridge, J. M., Bahreini, R., Cappa, C. D., Middlebrook, A. M., and Schwarz, J. P.: Brown carbon and internal mixing in biomass burning particles, *P. Natl. Acad. Sci. USA*, 109, 14802–14807, 2012.

Lanz, V. A., Alfara, M. R., Baltensperger, U., Buchmann, B., Hueglin, C., and Prévôt, A. S. H.: Source apportionment of submicron organic aerosols at an urban site by factor analytical modelling of aerosol mass spectra, *Atmos. Chem. Phys.*, 7, 1503–1522, doi:10.5194/acp-7-1503-2007, 2007.

Liu, S., Russell, L. M., Sueper, D. T., and Onasch, T. B.: Organic particle types by single-particle measurements using a time-of-flight aerosol mass spectrometer coupled with a light scattering module, *Atmos. Meas. Tech.*, 6, 187–197, doi:10.5194/amt-6-187-2013, 2013.

Massoli, P., Fortner, E. C., Canagaratna, M. R., Williams, L. R., Zhang, Q., Sun, Y., Schwab, J. J., Trimborn, A., Onasch, T. B., Demerjian, K. L., Kolb, C. E., Worsnop, D. R., and Jayne, J. T.: Pollution gradients and chemical characterization of particulate matter from vehicular traffic near major roadways: results from the 2009 Queens College Air Quality Study in NYC, *Aerosol Sci. Tech.*, 46, 1201–1218, 2012.

Matthew, B. M., Middlebrook, A. M., and Onasch, T. B.: Collection efficiencies in an Aerodyne Aerosol Mass Spectrometer as a function of particle phase for laboratory generated aerosols, *Aerosol Sci. Tech.*, 42, 884–898, 2008.

McMeeking, G. R., Good, N., Petters, M. D., McFiggans, G., and Coe, H.: Influences on the fraction of hydrophobic and hydrophilic black carbon in the atmosphere, *Atmos. Chem. Phys.*, 11, 5099–5112, doi:10.5194/acp-11-5099-2011, 2011.

Metcalf, A. R., Loza, C. L., Coggon, M. M., Craven, J. S., Jonsson, H. H., Flagan, R. C., and Seinfeld, J. H.: Secondary organic aerosol coating formation and evaporation: chamber studies using black carbon seed aerosol and the Single-Particle Soot Photometer, *Aerosol Sci. Tech.*, 47, 326–347, 2013.

Mohr, C., Huffman, J. A., Cubison, M. J., Aiken, A. C., Docherty, K. S., Kimmel, J. R., Ulbrich, I. M., Hannigan, M., and Jimenez, J. L.: Characterization of primary organic aerosol emissions from meat cooking, trash burning, and motor vehicles with high-resolution aerosol mass spectrometry and comparison with ambient and chamber observations, *Environ. Sci. Technol.*, 43, 2443–2449, 2009.

Single particle
characterization

A. K. Y. Lee et al.

Title Page

Abstract

Introduction

Conclusions

References

Tables

Figures



Back

Close

Full Screen / Esc

Printer-friendly Version

Interactive Discussion



- Mohr, C., DeCarlo, P. F., Heringa, M. F., Chirico, R., Slowik, J. G., Richter, R., Reche, C., Alastuey, A., Querol, X., Seco, R., Peñuelas, J., Jiménez, J. L., Crippa, M., Zimmermann, R., Baltensperger, U., and Prévôt, A. S. H.: Identification and quantification of organic aerosol from cooking and other sources in Barcelona using aerosol mass spectrometer data, *Atmos. Chem. Phys.*, 12, 1649–1665, doi:10.5194/acp-12-1649-2012, 2012.
- Moteki, N. and Kondo, Y.: Effects of mixing state on black carbon measurements by laser-induced incandescence, *Aerosol Sci. Tech.*, 41, 398–417, 2007.
- Ng, N. L., Canagaratna, M. R., Zhang, Q., Jimenez, J. L., Tian, J., Ulbrich, I. M., Kroll, J. H., Docherty, K. S., Chhabra, P. S., Bahreini, R., Murphy, S. M., Seinfeld, J. H., Hildebrandt, L., Donahue, N. M., DeCarlo, P. F., Lanz, V. A., Prévôt, A. S. H., Dinar, E., Rudich, Y., and Worsnop, D. R.: Organic aerosol components observed in Northern Hemispheric datasets from Aerosol Mass Spectrometry, *Atmos. Chem. Phys.*, 10, 4625–4641, doi:10.5194/acp-10-4625-2010, 2010.
- Onasch, T. B., Trimborn, A., Fortner, E. C., Jayne, J. T., Kok, G. L., Williams, L. R., Davidovits, P., and Worsnop, D. R.: Soot Particle Aerosol Mass Spectrometer: development, validation, and initial application, *Aerosol Sci. Tech.*, 46, 804–817, 2012.
- Pagels, J., Dutcher, D. D., Stolzenburg, M. R., McMurry, P. H., Gaelli, M. E., and Gross, D. S.: Fine-particle emissions from solid biofuel combustion studied with single-particle mass spectrometry: identification of markers for organics, soot, and ash components, *J. Geophys. Res.-Atmos.*, 118, 859–870, 2013.
- Pratt, K. A. and Prather, K. A.: Mass spectrometry of atmospheric aerosols: recent developments and applications, Part II: On-line mass spectrometry techniques, *Mass Spectrom. Rev.*, 31, 17–48, 2012.
- Schwarz, J. P., Gao, R. S., Fahey, D. W., Thomson, D. S., Watts, L. A., Wilson, J. C., Reeves, J. M., Darbeheshti, M., Baumgardner, D. G., Kok, G. L., Chung, S. H., Schulz, M., Hendricks, J., Lauer, A., Kaercher, B., Slowik, J. G., Rosenlof, K. H., Thompson, T. L., Langford, A. O., Loewenstein, M., and Aikin, K. C.: Single-particle measurements of midlatitude black carbon and light-scattering aerosols from the boundary layer to the lower stratosphere, *J. Geophys. Res.-Atmos.*, 111, D16207, doi:10.1029/2006JD007076, 2006.
- Shiraiwa, M., Kondo, Y., Moteki, N., Takegawa, N., Miyazaki, Y., and Blake, D. R.: Evolution of mixing state of black carbon in polluted air from Tokyo, *Geophys. Res. Lett.*, 34, L16803, doi:10.1029/2007GL029819, 2007.

Single particle
characterization

A. K. Y. Lee et al.

Title Page

Abstract

Introduction

Conclusions

References

Tables

Figures



Back

Close

Full Screen / Esc

Printer-friendly Version

Interactive Discussion



- Shiraiwa, M., Kondo, Y., Iwamoto, T., and Kita, K.: Amplification of light absorption of black carbon by organic coating, *Aerosol Sci. Tech.*, 44, 46–54, 2010.
- Slowik, J., Stainken, K., Davidovits, P., Williams, L., Jayne, J., Kolb, C., Worsnop, D., Rudich, Y., DeCarlo, P., and Jimenez, J.: Particle morphology and density characterization by combined mobility and aerodynamic diameter measurements, Part 2: Application to combustion-generated soot aerosols as a function of fuel equivalence ratio, *Aerosol Sci. Tech.*, 38, 1206–1222, 2004.
- Stephens, M., Turner, N., and Sandberg, J.: Particle identification by laser-induced incandescence in a solid-state laser cavity, *Appl. Optics*, 42, 3726–3736, 2003.
- Tritscher, T., Juranyi, Z., Martin, M., Chirico, R., Gysel, M., Heringa, M. F., DeCarlo, P. F., Sierau, B., Prevot, A. S. H., Weingartner, E., and Baltensperger, U.: Changes of hygroscopicity and morphology during ageing of diesel soot, *Environ. Res. Lett.*, 6, 034026, doi:10.1088/1748-9326/6/3/034026, 2011.
- Ulbrich, I. M., Canagaratna, M. R., Zhang, Q., Worsnop, D. R., and Jimenez, J. L.: Interpretation of organic components from Positive Matrix Factorization of aerosol mass spectrometric data, *Atmos. Chem. Phys.*, 9, 2891–2918, doi:10.5194/acp-9-2891-2009, 2009.
- Wang, J., Cubison, M. J., Aiken, A. C., Jimenez, J. L., and Collins, D. R.: The importance of aerosol mixing state and size-resolved composition on CCN concentration and the variation of the importance with atmospheric aging of aerosols, *Atmos. Chem. Phys.*, 10, 7267–7283, doi:10.5194/acp-10-7267-2010, 2010.
- Willis, M. D., Lee, A. K. Y., Onasch, T. B., Fortner, E. C., Williams, L. R., Lambe, A. T., Worsnop, D. R., and Abbatt, J. P. D.: Collection efficiency of the Soot-Particle Aerosol Mass Spectrometer (SP-AMS) for internally mixed particulate black carbon, *Atmos. Meas. Tech. Discuss.*, 7, 5223–5249, doi:10.5194/amtd-7-5223-2014, 2014.
- Zhang, Q., Jimenez, J. L., Canagaratna, M. R., Allan, J. D., Coe, H., Ulbrich, I., Alfarra, M. R., Takami, A., Middlebrook, A. M., Sun, Y. L., Dzepina, K., Dunlea, E., Docherty, K., DeCarlo, P. F., Salcedo, D., Onasch, T., Jayne, J. T., Miyoshi, T., Shimojo, A., Hatakeyama, S., Takegawa, N., Kondo, Y., Schneider, J., Drewnick, F., Borrmann, S., Weimer, S., Demerjian, K., Williams, P., Bower, K., Bahreini, R., Cottrell, L., Griffin, R. J., Rautiainen, J., Sun, J. Y., Zhang, Y. M., and Worsnop, D. R.: Ubiquity and dominance of oxygenated species in organic aerosols in anthropogenically-influenced Northern Hemisphere midlatitudes, *Geophys. Res. Lett.*, 34, L13801, doi:10.1029/2007GL029979, 2007.

Zhang, Q., Jimenez, J. L., Canagaratna, M. R., Ulbrich, I. M., Ng, N. L., Worsnop, D. R., and Sun, Y.: Understanding atmospheric organic aerosols via factor analysis of aerosol mass spectrometry: a review, *Anal. Bioanal. Chem.*, 401, 3045–3067, 2011.

5 Zhang, R., Khalizov, A. F., Pagels, J., Zhang, D., Xue, H., and McMurry, P. H.: Variability in morphology, hygroscopicity, and optical properties of soot aerosols during atmospheric processing, *P. Natl. Acad. Sci. USA*, 105, 10291–10296, 2008.

Single particle characterization

A. K. Y. Lee et al.

Title Page

Abstract

Introduction

Conclusions

References

Tables

Figures



Back

Close

Full Screen / Esc

Printer-friendly Version

Interactive Discussion



Single particle
characterization

A. K. Y. Lee et al.

Title Page

Abstract

Introduction

Conclusions

References

Tables

Figures

I◀

▶I

◀

▶

Back

Close

Full Screen / Esc

Printer-friendly Version

Interactive Discussion

**Table 2.** Summary of the rBC contribution to each cluster.

Cluster type	% of particles with measurable m/z 36 ¹ signal (# of particles)			Mass fraction of rBC (IR laser on) ²
	Laser on	Laser off	Difference (laser on minus off)	
NO ₃	11.4 % (1063)	10.2 % (652)	1.2 %	0.035
SO ₄	4.4 % (130)	2.8 % (67)	1.6 %	0.019
HOA	8.4 % (347)	2.0 % (65)	6.4 %	0.024
rBC	97.1 % (867)	NA	NA	0.722
COA	6.5 % (548)	2.9 % (205)	3.6 %	0.020
OOA 1	8.2 % (587)	4.1 % (291)	4.1 %	0.027
OOA 2	7.4 % (153)	3.9 % (80)	3.5 %	0.028

¹ IR laser on mode: m/z 36 = C₃⁺ and HCl⁺, IR laser off mode: m/z 36 = HCl⁺ only.² The fragmentation table shown in Table S2 in the Supplement was used for quantification of rBC

Single particle
characterization

A. K. Y. Lee et al.

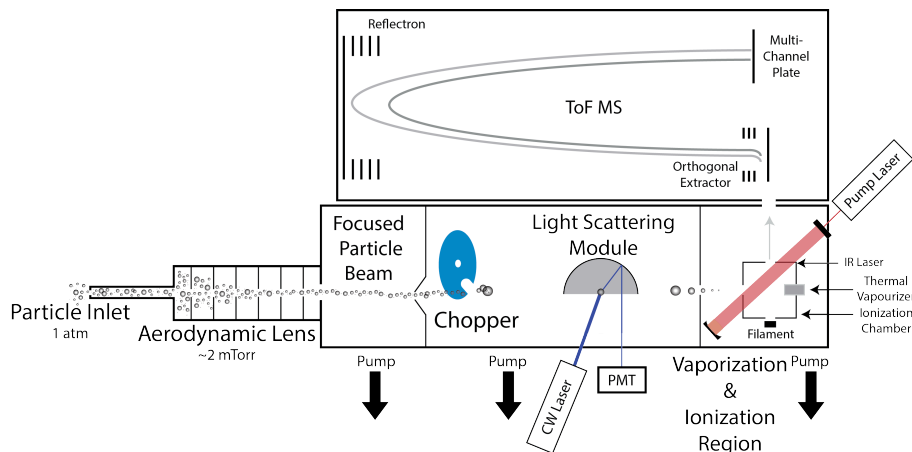


Figure 1. A simplified schematic of the SP-AMS equipped with a light scattering module (LS-SP-AMS) for ensemble measurements and single particle detection.

[Title Page](#)[Abstract](#)[Introduction](#)[Conclusions](#)[References](#)[Tables](#)[Figures](#)[◀](#)[▶](#)[◀](#)[▶](#)[Back](#)[Close](#)[Full Screen / Esc](#)[Printer-friendly Version](#)[Interactive Discussion](#)

Single particle
characterization

A. K. Y. Lee et al.

Title Page

Abstract

Introduction

Conclusions

References

Tables

Figures



Back

Close

Full Screen / Esc

Printer-friendly Version

Interactive Discussion

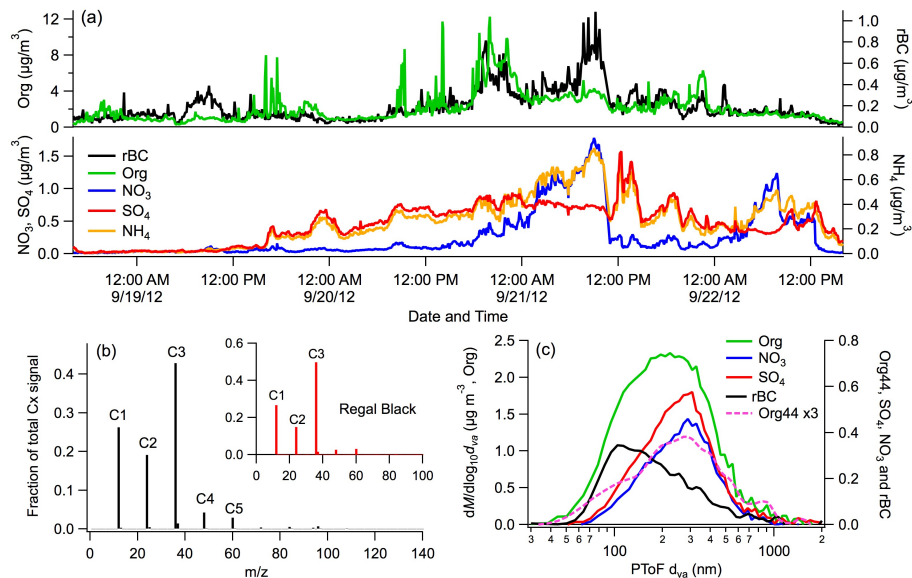


Figure 2. (a) Time series of laser off (Org, NO₃, SO₄, NH₄) and laser on (rBC) aerosol compositions. (b) The average mass spectrum of laser on ambient rBC and Regal Black (insert). (c) Average size distributions of laser off (Org, NO₃, SO₄, Org44) and laser on (rBC) aerosol compositions.

Single particle characterization

A. K. Y. Lee et al.

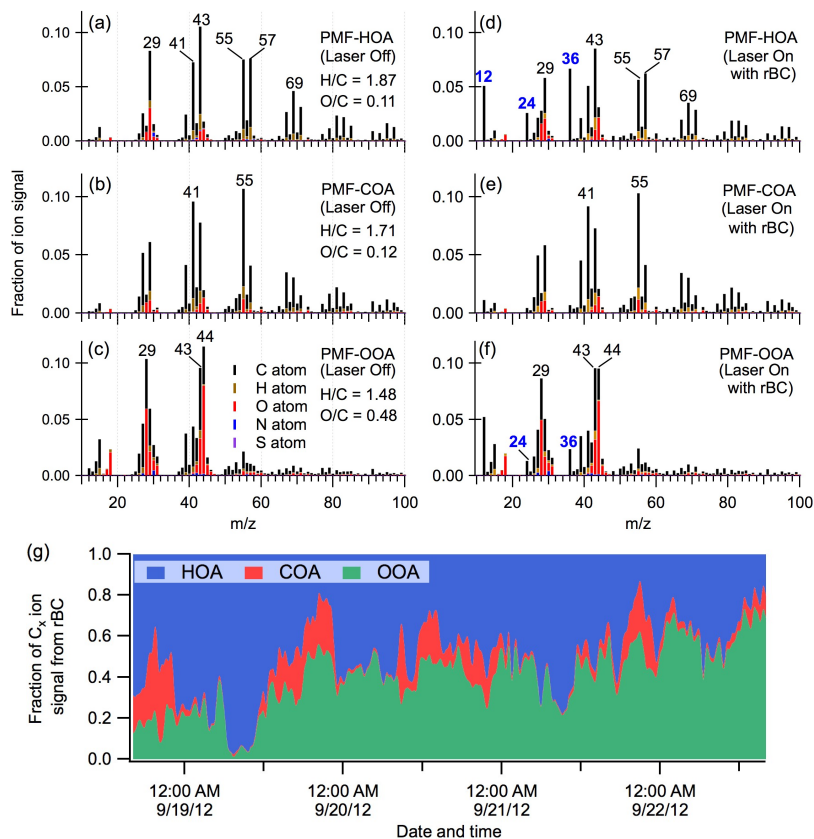


Figure 3. Normalized mass spectra of PMF factors from laser off (a–c) and laser on with rBC signals (d–f) mode measurements: (a and d) HOA factor, (b and e) COA factor, (c and f) OOA factor. (g) Mass fraction contribution of total C_x signal from each laser on mode PMF factor (d–f).

Single particle
characterization

A. K. Y. Lee et al.

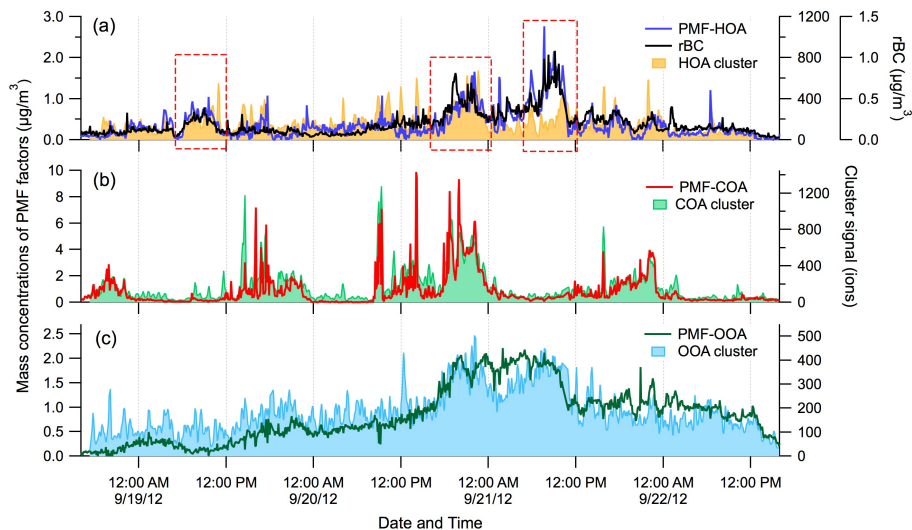


Figure 4. Time series profiles of rBC, PMF factors of organic components (from laser off mode MS measurements) and different organic clusters (from laser on mode LSSP measurements).

[Title Page](#)[Abstract](#)[Introduction](#)[Conclusions](#)[References](#)[Tables](#)[Figures](#)[Back](#)[Close](#)[Full Screen / Esc](#)[Printer-friendly Version](#)[Interactive Discussion](#)

Single particle characterization

A. K. Y. Lee et al.

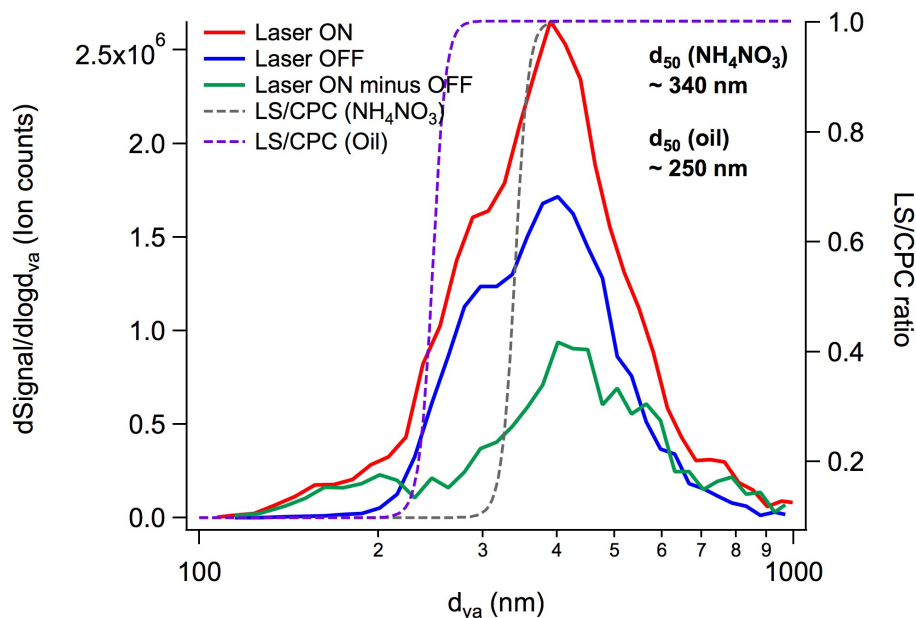


Figure 5. Size distributions of total ion counts from the ambient single particle measurements (red: laser on mode, blue: laser off mode, green: difference between laser on and laser off modes). The grey dashed line represents the counting efficiency (the ratio of light scattering counts and condensation particle counter signals (LS/CPC), left axis) of the light scattering module for ammonium nitrate particles. The purple dashed line indicates an estimated light scattering cut-off d_{va} for spherical hydrocarbon oil droplets (i.e., shape factor = 1 and density = 1 g cm^{-3}).

Title Page

Abstract

Introduction

Conclusions

References

Tables

Figures



Back

Close

Full Screen / Esc

Printer-friendly Version

Interactive Discussion



Single particle
characterization

A. K. Y. Lee et al.

Title Page

Abstract

Introduction

Conclusions

References

Tables

Figures

◀

▶

◀

▶

Back

Close

Full Screen / Esc

Printer-friendly Version

Interactive Discussion

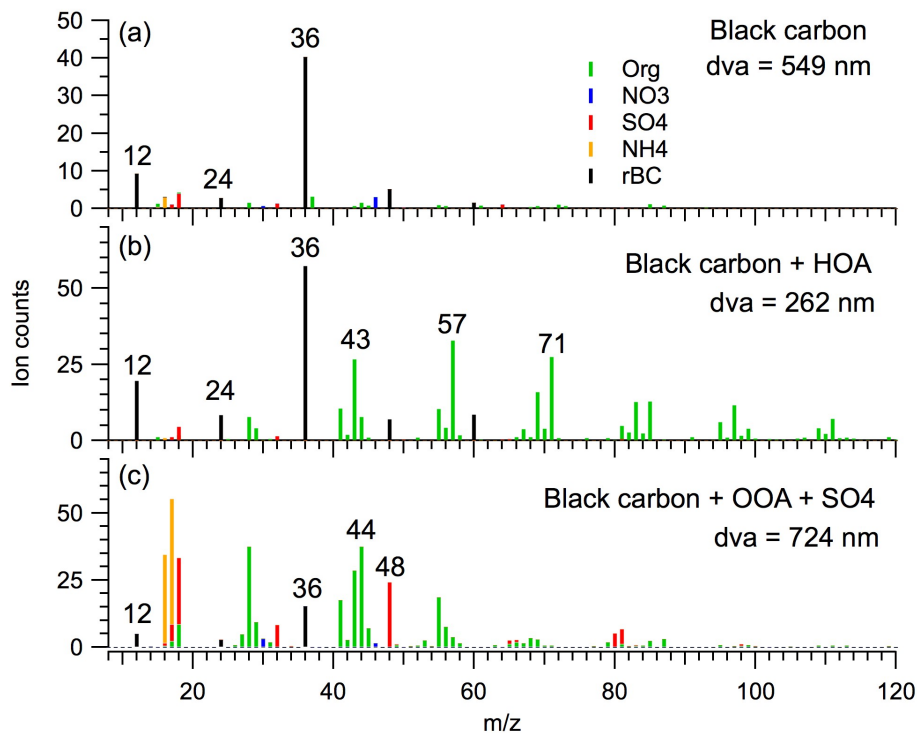


Figure 6. Examples of single particle mass spectra of rBC-containing particles: **(a)** black carbon, **(b)** black carbon with thin HOA coating, and **(c)** black carbon with OOA and sulfate coating. Particles **(a)** and **(b)** are sorted into the rBC cluster, and particle **(c)** are classified into the OOA cluster 2 identified in this study (see Sect. 3.5).

Single particle characterization

A. K. Y. Lee et al.

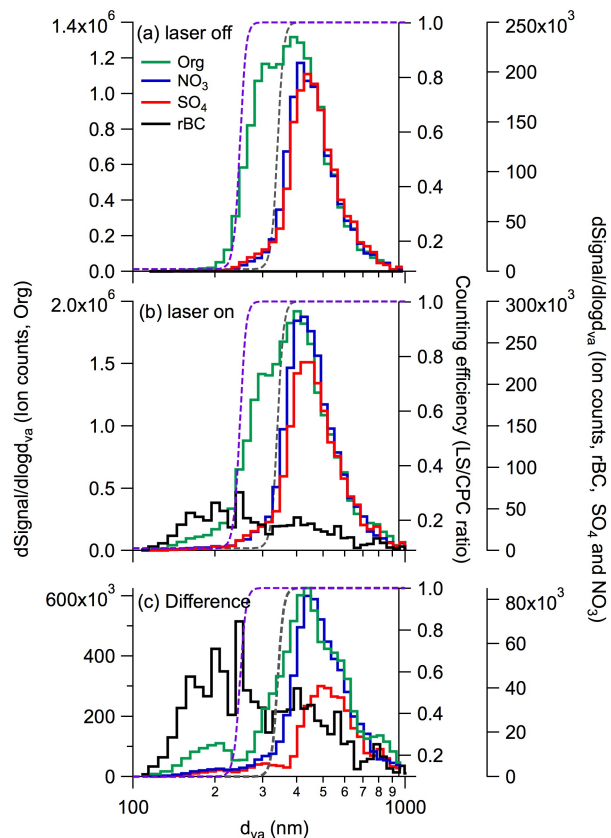


Figure 7. Size distributions of nitrate, sulfate, organics and rBC from the single particle measurements with IR laser off **(a)** and on **(b)** measurements. **(c)** Differences between laser on and off modes (i.e., laser on minus laser off data). The grey dashed line represents the counting efficiency (LS/CPC) of the light scattering module for ammonium nitrate particles. The purple dashed line indicates an estimated light scattering cut-off d_{va} for spherical hydrocarbon oil droplets.

Single particle
characterization

A. K. Y. Lee et al.

Title Page

Abstract

Introduction

Conclusions

References

Tables

Figures



Back

Close

Full Screen / Esc

Printer-friendly Version

Interactive Discussion

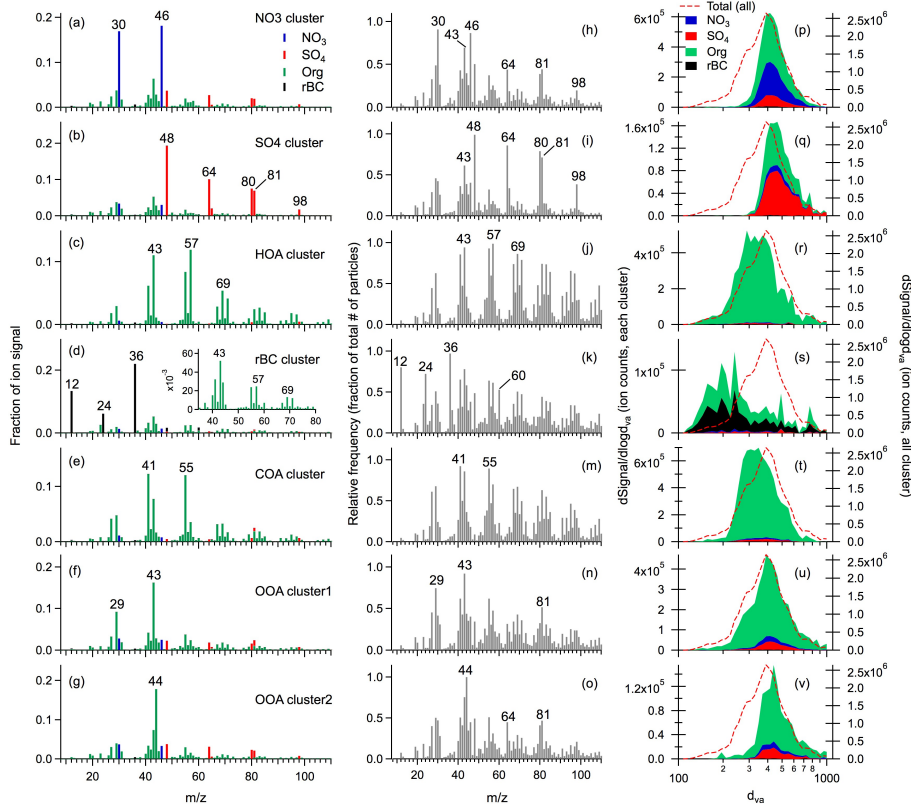


Figure 8. Normalized mass spectra (left column), normalized histograms displaying the relative frequency of each m/z (middle column), and size distributions (right column) of different clusters: (a, h and p) NO₃ cluster, (b, i and q) SO₄ cluster, (c, j and r) HOA cluster, (d, k and s) rBC cluster, (e, m and t) COA cluster, (f, n and u) OOA cluster1 – less oxygenated, (g, o and v) OOA cluster2 – more oxygenated.